JCI insight

REP1-deficiency causes systemic dysfunction of lipid metabolism and oxidative stress in choroideremia

Dulce Lima Cunha, … , Ailsa A. Welch, Mariya Moosajee

JCI Insight. 2021. https://doi.org/10.1172/jci.insight.146934.

Research In-Press Preview Metabolism Ophthalmology

Graphical abstract

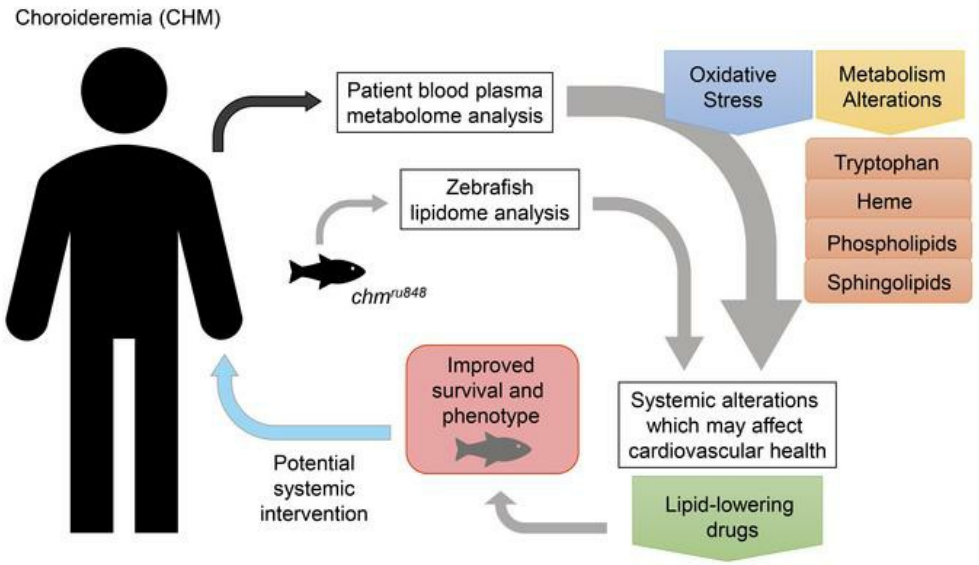

REP1-deficiency causes systemic dysfunction of lipid metabolism and oxidative stress in choroideremia

Authors: Dulce Lima Cunha[1], Rose Richardson[1], Dhani Tracey-White[1], Alessandro Abbouda[1,2], Andreas Mitsios[1,2], Verena Horneffer-van der Sluis[3], Panteleimon Takis[3], Nicholas Owen[1], Jane Skinner[4], Ailsa A Welch[4], Mariya Moosajee[1,2,5,6]

Affiliations:

1 – Department of Development, Ageing and Disease, UCL Institute of Ophthalmology, London, UK

2 – Department of Genetics, Moorfields Eye Hospital NHS Foundation Trust, London, UK

3- MRC-NIHR National Phenome Centre, Department of Surgery and Cancer, Imperial College London, London W120NN, UK

4 - Department of Public Health & Primary Care, Norwich Medical School, Norfolk, UK

5 - Department of Ophthalmology, Great Ormond Street Hospital for Children NHS Foundation Trust, London, UK

6 – The Francis Crick Institute, London, UK

Corresponding author:

Professor Mariya Moosajee MBBS, BSc, PhD, FRCOphth

UCL Institute of Ophthalmology

11-43 Bath Street

EC1V 9EL London

Tel: 020 7608 6851

Email: m.moosajee@ucl.ac.uk

Abstract

Choroideremia (CHM) is a X-linked recessive chorioretinal dystrophy caused by mutations in *CHM*, encoding for Rab escort protein 1 (REP1). Loss of functional REP1 leads to the accumulation of unprenylated Rab proteins and defective intracellular protein trafficking, the putative cause for photoreceptor, retinal pigment epithelium (RPE) and choroidal degeneration. *CHM* is ubiquitously expressed, but adequate prenylation is considered to be achieved, outside the retina, through the isoform REP2. Recently, the possibility of systemic features in CHM has been debated, hence, in this study whole metabolomic analysis of plasma samples from 25 CHM patients versus age and gender matched controls was performed. Results showed plasma alterations in oxidative stress-related metabolites, coupled with alterations in tryptophan metabolism leading to significantly raised serotonin levels. Lipid metabolism was disrupted with decreased branched fatty acids and acylcarnitines, suggestive of dysfunctional lipid oxidation, and imbalances of several sphingolipids and glycerophospholipids. Targeted lipidomics of the *chm*^{ru848} zebrafish provided further evidence for dysfunction, with the use of Fenofibrates over Simvastatin circumventing the prenylation pathway to improve the lipid profile and increase survival. This study provides strong evidence for systemic manifestations of CHM and proposes novel pathomechanisms and targets for therapeutic consideration.

Introduction

Choroideremia (CHM, OMIM 303100) is a chorioretinal dystrophy, with an incidence of 1 in 50,000-100,000, characterised by the progressive degeneration of photoreceptors (PR), retinal pigmented epithelium (RPE) and choroid (1, 2). Affected male patients typically suffer from nyctalopia in the first decade of life that progresses to severe peripheral field loss with complete blindness in late adulthood, with no reports of associated systemic features (3). CHM is a X-linked recessive, monogenic disorder caused by mutations in the *CHM* gene (OMIM 303390). *CHM* encodes Rab Escort Protein 1 (REP1), an essential component of the catalytic Rab geranyl-geranyl transferase II (GGTase II) complex, which is essential for prenylation of Rab GTPase proteins (4, 5). Protein prenylation is a type of post-translational lipid modification, which involves the covalent addition of either farnesyl- or geranylgeranyl-pyrophosphate (FPP or GGPP) to proteins via three different prenyltransferases: farnesyltransferase (FTase) and geranylgeranyl transferases (GGTase) I and II (4). REP1 and its isoform Rab Escort Protein 2 (REP2) recruit newly synthesized Rab GTPase proteins and present them to GGTase II, forming a tight catalytic complex in which two GGPP are transferred onto the C terminus. After prenylation, REP1/2 escorts the Rabs to their respective target membrane (6).

As *CHM* is ubiquitously expressed, the possibility of systemic manifestations has long been considered but remains unproven. It is accepted that REP2 compensates for the REP1 deficiency, providing adequate prenylation of Rab proteins in all extra-retinal tissues (7). Lack of this compensatory mechanism in the retina, due to preferential binding affinity of Rab27a, 6, 8 and 11 to REP1, is thought to lead to the accumulation of these unprenylated Rabs, resulting in an

isolated ocular phenotype (5). However, an online self-reporting survey of 190 individuals - CHM male patients (n=117), female carriers (n=53) and unaffected males (n=20) - undertaken by Zhou *et al*. suggested a higher prevalence of diabetes, high cholesterol and hyperglycemia in CHM male patients, but these differences were not significant after age adjustment (8). They suggested that hydroxy-3-methyl-glutaryl-CoA reductase (HMG-CoA) inhibitors (also known as statins) for the treatment of hypercholesterolemia may have a negative effect on the visual function of CHM patients (8). GGPP and FPP are both isoprenoids produced through the mevalonate pathway, which is the main pathway for cholesterol synthesis and the target of these drugs (9). It has recently been reported that statins lead to lower pools of both isoprenoids necessary for GGTases activity and consequent inhibition of both farnesyl and geranylgeranyl prenylation (10-13).

Previously, analysis of lipid contents from blood samples of 5 CHM patients uncovered systemic fatty acid (FA) abnormalities in both plasma and red blood cells (RBCs). Specifically, lower levels of eicosenoic acid (C20:1[n-9]), erucic acid (C22:1[n-9]), and docosadienoic acid (C22:2[n-6] were found in the plasma, with elevation of tridecaenoic acid (C13:1), myristolenic acid (C14:2), and octacosanoic acid (C28:0). RBCs revealed increased levels of capric acid (C10:0), nervonic acid (C24:1[n-9]), and plasmalogen derivative dimethylacetal acid (16:0), as well as a decrease in eicosenoic acid (C20:1[n-9]) (14). A follow-up report refuted these findings, stating no lipid abnormalities were detected in the plasma of 9 CHM patients, nor could crystal deposits be detected after transmission and scanning electron microscopy analyses of white blood cells and RBCs, respectively (15).

Herein, we performed whole metabolomic profiling of blood plasma from 25 CHM male patients and 25 age- and gender-matched controls to identify metabolic alterations in CHM and gain insights into any systemic involvement. Several pathways were significantly altered in the disease cohort including sphingolipid signal transduction, oxidative stress and serotonin production.

Zebrafish have been acknowledged as a valuable model for studying metabolism and metabolic diseases (16, 17). Accordingly, targeted lipidomics analysis of the CHM zebrafish model *chm*^{ru848}, with a C>T nonsense variant (p.(Gln32*)) in *chm* exon 2 on chromosome 21, confirmed lipid and sphingolipid alterations found in humans. Furthermore, we also undertook survival studies and lipidomic analysis of *chm*^{ru848} embryos treated with Simvastatin or Fenofibrate (a fibric acid derivative mediated via activation of Peroxisome Proliferator Activated Receptor type alpha [PPARα]) to explore if prenylation is affected by statins. Zebrafish possess only one rep isoform, which leads to retinal degeneration from 4.5 days post fertilisation (dpf) and multisystemic disease resulting in embryonic lethality by 5-6 dpf (18, 19).

This study discovers the metabolomic signature in CHM, and identifies putative disease biomarkers, which may be critical to the future development of disease-modifying or preventative therapies.

Results

PATIENT DESCRIPTION

Detailed clinical and genetic evaluation of 25 male CHM patients is included in Supplementary Table 1. Mean ± SD age of CHM patients at the time of blood collection was 40.6 ± 11.4 years (range 20-63 years), with no significant difference with the control group (40.7 ± 12.3 years, $p = 0.938$). Analysis of the food frequency questionnaire (FFQ) revealed no significant dietary differences between disease and control groups with regards to average consumption of food and drink over the past 12 months (Supplementary Table 2).

GLOBAL METABOLITE DIFFERENCES BETWEEN CHM PATIENTS AND CONTROLS

Eight hundred and seventeen compounds of known identity were detected in the blood plasma matrix of CHM patients and controls. Principle component analysis (PCA) of CHM patient and healthy control samples revealed largely overlapping grouping with no clear distinction between study groups (Figure 1A). Consistently, hierarchical cluster analysis of the dataset revealed the same trend, with interdigitated sample clustering for healthy control and CHM patient samples (Figure 1B). Welch's two-sample *t*-test was used to identify compounds that differed significantly between CHM and healthy control study groups, with 85 named compounds achieving statistical significance ($p \leq 0.05$) and a further 48 approaching significance ($0.05 < p < 0.10$).

INDIVIDUAL BIOCHEMICALS CAN DIFFERENTIATE BETWEEN CHM PATIENTS AND CONTROL STUDY GROUPS

Random forest (RF) analysis indicated high probability that individual metabolites can distinguish between study groups, with a predictive accuracy of 86%. The top 30 metabolites based on distinguishing CHM from control groups are represented in Figure 1C and in more detail in Supplementary Table 3. These include several sphingolipid signal transducers [sphingosine, sphingadienine, sphinganine, hexadecasphingosine (d16:10)*, sphinganine-1-phosphate, and sphingosine-1-phosphate]; Stearoyl-glycerophosphoserine (GPS) moieties for both lysolipids (e.g. 1-stearoyl-GPS [18:0]*), and phosphatidylserine (PS) derivatives (e.g. 1-stearoyl-2-arachidonoyl-GPS [18:0/20:4] and 1-stearoyl-2-oleoyl-GPS [18:0/18:1]). Additionally, several metabolites in the cysteine pathway (cysteine s-sulfate, cysteine, cysteinylglycine, cys-gly oxidized) were highlighted (Figure 1C).

Pathway set enrichment analysis to elucidate the metabolic pathways affected between CHM patients and controls revealed significant perturbation of multiple networks, including oxidative stress, tryptophan metabolism, haemoglobin metabolism and particularly sphingolipid and lipid metabolisms (Figure 1D).

CHM PATIENTS EXHIBIT EVIDENCE OF INCREASED OXIDATIVE STRESS

We observed mixed perturbations in the cysteine pathway (Figure 2A), such as loss of cysteine (FC 0.81, $p < 0.001$) (Figure 2B) and associated dipeptide cysteinylglycine (FC 0.56, $p < 0.001$) (Figure 2C), which may indicate an increased demand for the antioxidant glutathione. An elevation of oxidative stress

marker cys-gly oxidized (FC 1.35, $p < 0.01$) (Figure 2E) and increase of lipid oxidation marker 12,13-DiHOME (FC 1.31, $p < 0.05$) (Figure 2I) were also observed, coupled with an accumulation of hypotaurine (FC 1.53, $p < 0.01$) (Figure 2H). Several other known antioxidants were found in significantly lower levels in CHM samples, like bilirubin (FC 0.80, $p < 0.05$) (Figure 3I), indolepropionate (FC 0.40, $p < 0.05$) (Figure 3E), beta-cryptoxanthin (provitamin A) (FC 0.69, $p < 0.05$), urate (FC 0.87, $p < 0.05$) and suspected antioxidant 3-(3-hydroxyphenyl)propionate (FC 0.42, $p < 0.005$) (data not shown). Cysteine-s-sulfate is an incompletely characterised metabolite generated by reaction of cysteine and inorganic sulfite, and was greatly reduced in CHM plasma (FC 0.10, $p < 0.001$) (Figure 2D). This likely relates to increased sulfite oxidase (SO) activity, which catalyses the oxidation of sulfite to sulfate, the potentiation of which may divert away from cysteine-s-sulfate production (Figure 2A). Combined, these observations seem to point to a deficient management of oxidative stress in CHM patients, possibly through deregulation of gluthathione metabolism, although glutathione levels are not usually detected in plasma.

CHM PATIENTS DISPLAY ALTERATIONS IN TRYPTOPHAN METABOLISM

Tryptophan metabolism pathway was enriched in this study with a score of 1.62 (Figure 1D, 3A), with serotonin levels being strikingly elevated in CHM patients (FC 3.82, $p < 0.001$) (Figure 3B). Serotonin is an important monoaminergic neurotransmitter that regulates stress response, sleep, behaviour, amongst other body functions, and this increase indicates that tryptophan metabolism appears to be strongly shifted towards monoamine production. This observation is consistent with lower levels of alternative tryptophan catabolic pathways,

involving microbiome-related indolelactate (FC 0.79, $p < 0.05$) and indolepropionate (FC 0.40, $p < 0.05$) in CHM patients (Figure 3D, E). Also, there was no significant difference in nicotinamide levels between CHM and control samples (FC 1.02, $p = 0.96$) (not shown), although higher levels of quinolate (FC 1.45, $p < 0.05$) were detected (Figure 3C).

DEFECTS IN CYTOCHROME ACTIVITY

Haemoglobin synthesis and porphyrin metabolism pathway showed a high pathway enrichment score (6.67) in this study (Figure 1D). Although only 6 compounds were analysed overall (Figure 3F), we observed significantly lower levels of bilirubin isomers (Z, Z) (FC 0.82, $p < 0.05$) (Figure 3I), (E, Z or Z,E)* (FC 0.82, $p < 0.05$) and (E, E)* (FC 0.79, $p < 0.05$) (not shown), coupled to a trending reduction of its precursor biliverdin (FC 0.87, $p < 0.1$) in CHM samples (Figure 3H). In contrast, the product of bilirubin reduction, L-urobilin, was detected in higher levels (FC 2.53, $p < 0.01$) (Figure 3J). However, levels of heme were not significantly increased (FC 1.58, $p > 0.1$) (Figure 3G), suggesting alterations occur downstream in the pathway.

While altered levels of bilirubin and urobilin could indicate increased heme breakdown in CHM patients, broader evidence perhaps indicates lower liver cytochrome P450 activity. Cytochrome P450s metabolise several methylxanthines, which largely trend lower in CHM individuals, such as 3, 7-dimethylurate (FC 0.62, $p < 0.05$), 3-methylxanthine (FC 0.59, $p < 0.1$), caffeic acid sulfate (FC 0.61, $p < 0.1$), 7-methylurate (FC 0.48, $p < 0.1$), theobromine (FC 0.63, $p < 0.1$) and 7-methylxanthine (FC 0.60, $p < 0.1$) (not shown). Additionally, cytochrome P450s also catalyse steroid biosynthesis, and a trending decrease in

several steroid hormones and related metabolites in CHM patients was observed (Supplementary Figure 1), which further supports the hypothesis of impaired cytochrome activity in choroideremia patients.

CHM PATIENTS EXHIBIT DISRUPTION IN SPHINGOLIPID METABOLISM

Deeper analysis of the compounds identified by RF analysis revealed broader perturbation of the sphingolipid pathways in CHM patients (Figure 4). The sphingolipid pathway generates the bioactive lipid metabolite ceramide. Ceramides can be produced or utilized through three main pathways; *de novo* biosynthesis, sphingomyelinase (SMase) pathway, or via the salvage pathway (Figure 4A). We observed increased levels of 3-phosphoglycerate (FC 1.56, $p < 0.01$) (Figure 4B), a key component to initiate the *de novo* sphingolipid synthesis, along with several intermediates including sphinganine (FC 1.41, $p < 0.001$) (Figure 4C) and sphinganine-1-phosphate (FC 1.35, $p < 0.001$) (Figure 4D).

In the salvage pathway, sphingosine 1-phosphate (S1P) was significantly increased (FC 1.24, $p < 0.01$) (Figure 4F) as well as hexadecasphingosine (d16:1) (FC 1.32, $p < 0.01$) (Figure 4E). S1P is cleaved into hexadecanal, a fatty aldehyde, and phosphoethanolamine, the latter also increased in CHM patients (FC 1.40, $p < 0.01$) (Figure 4G); although hexadecanal was not detected in this study, its product, hexadecanoic acid (also called palmitic acid or palmitate), was not significantly altered in CHM patients (not shown).

A modest depletion of a number of sphingomyelins (SMs) was detected including SM(d18:1/20:0, d16:1/22:0) (FC 0.91, $p < 0.05$) (Figure 4H) and SM(d18:1/22:1, d16:1/24:1) (FC 0.92, $p < 0.05$) (Figure 4I). SMs are synthesized by the transfer

of a phosphorylcholine residue from phosphatidylcholine to a ceramide by sphingomyelin synthase. SMs can also be hydrolysed back to release ceramides and phosphorylcholine residues by the action of SMase (20). In accordance, several phosphatidylcholines (PC) were also detected in significant lower levels in CHM patients, such as PC(16:0/22:6) (FC 0.88, $p < 0.05$) and PC(18:1/22:6) (FC 0.87, $p < 0.05$) (not shown), implying phospholipid deregulation caused by REP1 deficiency.

Ceramide is considered the central molecule in the sphingolipid metabolic pathway. Surprisingly, none of the ceramides detected in this study showed significantly altered levels in CHM samples compared to controls (not shown). Overall, these results could suggest a compensatory mechanism, possibly mediated by REP2, to regulate the ceramide pool through an increase of both *de novo* and salvage pathways to possibly compensate the underperformance of the SMase pathway.

CHM PATIENTS EXHIBIT BROADER ALTERATIONS IN LIPID METABOLISM

Sphingolipid metabolism also contributes to glycerophospholipid metabolism and disruption of this pathway can reduce glycerolipid levels, leading to broader lipid metabolism alterations. We observed differential effects of glycerolipid subclasses, with lower levels of phosphatidylcholine (PC) intermediates (Figure 5A), but increased levels of phosphatidylethanolamine (PE) (Figure 5B) and phosphatidylserine (PS) lipids (Figure 5C). Of the latter group, two PS intermediates, 1-stearoyl-GPS(18:0) and 1-stearoyl-2-arachidonoyl-GPS(18:0/20:4) were particularly increased in CHM patients, with nearly 4- and 6-fold change compared to control samples, respectively (Figure 5C).

No major differences were found in CHM patients regarding long chain fatty acid (FA) levels, in contrast with the study from Zhang et al (13). However, reduced levels of branched FAs 17-methylstearate (i19:0) (FC 0.75, $p < 0.05$) and 15-methylpalmitate (i17:0) (FC 0.78, $p < 0.1$) were observed, as well as several dicarboxylic FAs (DCFAs) (Figure 5D) and acylcarnitines (Figure 5E). Combined, these results point to impaired lipid oxidation in CHM patients.

HUMAN CHM LIPID ALTERATIONS ARE RECAPITULATED IN *chm*^{ru848} ZEBRAFISH

LC-MS based lipid profiling of *chm*^{ru848} homozygous mutant zebrafish embryos at 6 days post fertilisation (dpf) further corroborated the alterations in lipid metabolism detected in the plasma of CHM patients. Lipidomic-based PCA showed a clear separation between wildtype (wt) and *chm*^{ru848} groups, which was not visible in the human analysis (Figure 6A). Twelve compounds were found with differential levels between *chm*^{ru848} and wildtype samples that were also in the top 30 biochemicals from the human study, such as lysophosphatidylserine (Lyso-PS) (18:0) (1-stearoyl-GPS) and sphingosine (d18:1/22:0) (lactosyl-N-behenoyl-sphingosine). These metabolites were increased in both human and zebrafish CHM models (Figure 6B, C). Metabolites found in significant lower levels in *chm*^{ru848} as well as in human CHM samples included SM(d16:1/22:0) (Figure 6F) and several PC compounds, i.e. PC(16:0/22:6), PC(18:0/18:2) and PC(18:1/22:6) (Figure 6G-I).

Sphingosine-1-phosphate (S1P) (Figure 6D), Bilirubin (Figure 6E), SM(d16:1/24:1) and SM (d18.2/22:0) (not shown) were detected in *chm*^{ru848}, but levels were not statistically significant compared to wt samples. In contrast,

carnitine (C18-DC) (Figure 6J) and diacylglycerol DG(16:0/16) (Figure 6K) were significantly increased and decreased, respectively, in *chm*^{ru848}, while the same compounds had opposite trends in the human study ($0.05 < p \leq 0.1$) (Figure 5E, not shown). These differences are likely due to the presence of a single REP isoform in zebrafish, resulting in complete loss of REP activity, compared to humans, which have the compensatory action of REP2.

SIMVASTATIN VERSUS FENOFIBRATE TREATMENT IN *chm*^{ru848}

As the lipid profile in both humans and zebrafish with CHM show disruption, the effect of HMG-CoA reductase inhibitors (also known as statins) and fibric acid derivatives (fibrates) were investigated using the zebrafish model. Statins have been shown to block the mevalonate pathway necessary for cholesterol synthesis, the same pathway necessary to produce isoprenoids essential for prenylation and REP1 function (9). Hence, in an already compromised system, we wanted to investigate if fibrates (whose mode of action circumvents the mevalonate pathway) would be a safer compound to aid in normalising lipid dysregulation without exacerbating the underlying biochemical genetic defect in CHM and potentially accelerating their retinal phenotype.

We administered pre-determined doses of 0.3nM Simvastatin and 700nM Fenofibrate to wt and *chm*^{ru848} mutant fish (n=3, 50 embryos per group) from 24 hours, replenished daily till 9 days post fertilisation (dpf). There were no adverse side effects seen in treated wt embryos, all demonstrating normal stereotyped motor behaviours that allowed them to navigate their environment including slow and fast swimming bouts, with no signs of imbalance or lack of movement.

317 Characterisation of untreated and treated *chm*^{ru848} is presented in Figure *7.*
318 Survival studies showed untreated mutant zebrafish mean survival was 4.5 ± 0.5
319 days, while fish treated daily with Simvastatin survived 6.8 ± 0.4 days and those
320 with daily Fenofibrate survived 7.8 ± 0.5 days (Figure 7A). Cholesterol levels were
321 measured by Amplex Red Cholesterol Assay kit, which suggested a trend
322 increase in mutant compared to wildtype fish (p = 0.032). Simvastatin- and
323 Fenofibrate-treated mutants both showed comparable reduction of cholesterol
324 levels compared to untreated fish, although only the Fenofibrate-treated group
325 showed a significant reduction (p = 0.048) (Figure 7B). Histological analysis of
326 *chm*^{ru848} eyes at 6 dpf showed microphthalmia, cataract, and widespread retinal
327 degeneration with loss of lamination and areas of RPE hypertrophy/atrophy
328 (Figure 7C). Wholemount analysis of *chm*^{ru848} embryos showed characteristic
329 systemic defects including pericardial and abdominal oedema, an uninflated
330 swim bladder and persistent yolk sac (Figure 7C) (21). Following treatment, no
331 obvious phenotypic improvement was detected in Simvastatin-treated retinas,
332 while Fenofibrate-treated mutants showed clearer retinal lamination and
333 strikingly, with improved lens structure, although areas with significant RPE
334 atrophy were still present (Figure 7C).
335
336 We then performed targeted lipidomic analysis of *chm*^{ru848} mutant fish treated
337 with 0.3nM Simvastatin or 700nM Fenofibrate, compared to untreated mutants
338 and wildtype fish. PCA results show no clear distinction between treated groups
339 and untreated *chm*^{ru848} fish (Figure 6A).
340 The effect of Simvastatin on *chm*^{ru848} mutant fish leads to a decrease of Lyso-
341 PS(18:0) (Figure 6B) and PC(18:1/22:6) (Figure 6I), but the remaining

metabolites showed no significant changes between Simvastatin-treated and untreated groups. Fibrates are PPAR-alpha agonist lipid-lowering drugs that seem to have a broader effect in lowering overall lipid levels compared to statins (22). Consistently, *chm* fish treated with 700nM Fenofibrate showed lower levels of most compounds selected in this lipidomics analysis compared to untreated *chm*^{ru848} samples; metabolites that were already decreased in untreated mutant samples, particularly SMs (Figure 6F) and PCs (Figure 6G-I) and were reduced further. These compounds were largely unchanged by Simvastatin, confirming the different modes of action between the two drugs. However, it must be mentioned that there was a high variability in Fenofibrate-treated *chm* zebrafish, suggesting these results need further analysis or require a larger sample number to reduce variability and reach significance.

Discussion

This is the first study to explore systemic disturbances in choroideremia through whole metabolomic analysis of blood plasma from 25 CHM patients and 25 age- and gender-matched controls using Ultrahigh Performance Liquid Chromatography-Tandem Mass Spectrometry (UPLS-MS). Global analysis of the metabolomic data identified several biochemicals which can be adopted as biomarkers to distinguish between the two groups including 1-steroyl-GPS and lactosyl-N-behenoyl-sphingosine. Pathway enrichment analysis highlighted significant alterations in CHM patients, the key pathways being lipid metabolism, particularly sphingolipid metabolism, cysteine and glutathione metabolism, tryptophan metabolism and heme metabolism.

Sphingolipids are involved in different cellular processes and can have opposing effects; ceramides and sphinganines are considered pro-apoptotic and can mediate apoptosis, growth arrest and senescence. In contrast, S1P is associated with cell proliferation, migration and inflammation, and sphingomyelins (SM) are linked to cell growth and adhesion (20, 23). In the eye, oxidative stress is shown to increase ceramide and sphingosine levels, leading to photoreceptor death and RPE degradation, while S1P acts as a mediator of PR survival, preventing PR death during development and when exposed to oxidative stress (24). Analysis of sphingolipid metabolism revealed substantial imbalances in the presumptive ceramide pathway in CHM plasma, with increased levels of several sphinganines and sphingosines, including S1P, in parallel with lower levels of sphingomyelins, suggesting compromised ceramide production via the sphingomyelinase pathway. It is unclear if these findings correlate with the retinal environment and

disease severity, but measuring sphingolipid levels in photoreceptors and RPE derived from CHM patients, such as through generation of patient-derived induced pluripotent stem cells, may provide novel information on the effect of these metabolites in disease pathophysiology.

Sphingolipid metabolism perturbations can also suggest compromised degradation of the S1P pathway, that catalyses the conversion of hexadecanal to hexadecanoic acid. Interestingly, this pattern is similar to metabolic perturbations identified in Sjögren-Larsson syndrome (SLS) (OMIM 270200), an autosomal-recessive, neurocutaneous disease characterised by ichthyosis, mental retardation and spastic diplegia (25). SLS is caused by mutations in the *ALDH3A2* gene which encodes the membrane-bound fatty aldehyde dehydrogenase (FALDH), that catalyses the dehydrogenation of hexadecanal in the S1P degradation pathway (26). FALDH is present in the retina, RPE and choroid (27), with ocular defects recently identified in SLS patients including perifoveal crystalline inclusions, RPE atrophy with lipofuscin granules, retinal thinning and deficient macular pigment (28). Given the similar perturbations between diseases, we hypothesize that FALDH could also be a target for REP1, as it also has been found to require prenylation for proper localisation and function (10). In fact, other aldehyde dehydrogenases, ALDH3B1 and ALDH3B2, are also reported to be prenylated, through both farnesylation and geranylgeranylation (29, 30).

Analysis of specific metabolites related to lipid metabolism pointed to disruption of different phospholipid classes. For example, while a reduction of

phosphotidylcholine (PC) intermediates in CHM patients was detected, we also observed increased levels of some phosphatidylethanolamines (PE) and, particularly high accumulation of phosphatidylserine (PS) lipids. These different phospholipid subclasses are metabolically and structurally similar; PS is synthesized by PS synthases 1 and 2 in the endoplasmic reticulum (ER), that exchange serine for choline or ethanolamine in PC or PE, respectively. Conversely, PS can be converted to PE by phosphatidylserine decarboxylase (PSD) in the mitochondria (31). These observations may imply decrease activity of these enzymes, particularly PSD. Increased PS levels have not been associated with any human phenotype to date, but PS are increased in neuronal cells through docosahexaenoic acid (DHA), inhibiting neuronal cell death (32). However, levels of DHA in choroideremia were not significantly altered (FC 0.72, $p > 0.1$). PS can also result from phospholipase A-type enzymatic activity; this is a massive enzymatic family involved not only in phospholipid remodelling but also in cholesterol metabolism, cell differentiation, maintenance of mitochondrial integrity, cell proliferation and cell death (33). Interestingly, some phospholipase A enzymes have also been described as essential for RPE survival and regulation of POS phagocytosis (34, 35) and tightly linked to protein prenylation (36).

Unlike Zhang et al, no significant differences in saturated FAs, mono or polyunsaturated FAs were detected in our cohort (14), except for a reduction of branched FA 17-methylstearate (i19:0). These results were in accordance to the study by Radziwon et al, who did not detect FA metabolism differences in a cohort of 9 CHM patients (15). Nervonic acid, the only FA altered in CHM patients in both studies, was not detected through UPLS-MS. However, we observed

reduced levels of a few dicarboxylated FAs (DCFAs) as well as lower levels of acylcarnitines, which, combined with a trend reduction of branched FAs, may suggest impaired lipid beta oxidation.

Through targeted lipidomic analysis, we show that the zebrafish CHM model, *chm*^{ru848}, also presents distinct lipid profiles to the wt zebrafish. It should be noted that absence of rep1 in *chm*^{ru848}, coupled with the evolutionary lack of a compensatory rep2 isoform in zebrafish, results in a very severe systemic phenotype that leads to embryonic lethality by 5-6 dpf. This contrasts with the human form of the disease, and may have a global influence on the metabolic parameters. However, systemic lipid abnormalities are characterised by overall decreased levels of several PC and SM, which are recapitulated in the CHM patient plasma. Accordingly, 1-steroyl-GPS is significantly increased in *chm*^{ru848}, highlighting this compound as a putative novel biomarker for choroideremia, although its role and relation to CHM has not been uncovered yet.

Several recent studies have described the inhibitory effect of statins on the isoprenoid pathway as well as on prenylation of several Rab proteins, namely Rab7 (10-12). The *chm*^{ru848} zebrafish model showed a trend increase of cholesterol levels that were reduced following treatment with both statins and fibrates. Overall survival was increased in both drug treated mutants, however the Fenofibrate-treated eyes showed a mild rescue with increased overall eye size and a less compacted lens. Interestingly, it was suggested that prenylation of GTP-binding proteins is also necessary for lens homeostasis (37). Coincidently, statins (lovastatin) treatment induced cataract formation in cultured

rat lenses, which was alleviated by addition of GGPP (13), reinforcing the evidence that statins reduce the GGPP pool in the mevalonate pathway, making its use less indicated for CHM patients. We can also suggest that rep1 deficiency causes cataract formation in fish likely due to deficient prenylation. Patients with CHM develop posterior subcapsular cataracts, however the cause of this remains unclear. In retinitis pigmentosa, increased aqueous flare (which is related to the amount of protein present from increased breakdown of the blood-retinal-barrier and inflammation) has been found in patients with posterior subcapsular cataracts, potentially suggesting a similar inflammatory mechanism in CHM (38, 39). Considering the broad action of PPAR alpha agonists, the mechanism by which Fenofibrate-treatment potentially reduces cataract formation in the *chm*^{ru848} embryos is not fully understood, but may be through lowering cholesterol levels, which can cause cataracts when disturbed (40). However, Simvastatin-treated lenses showed no improvement, although overall cholesterol levels were also lower after treatment. It is therefore important to clarify the mechanism of action of Fenofibrates in *chm*^{ru848} zebrafish, since, considering the improvement of the ocular phenotype of mutant fish as well as its overall increased survival and lower cholesterol levels, Fenofibrate (and perhaps other PPAR alpha agonists) could have some therapeutic potential for CHM.

In 2012, a phase 1/2 trial was initiated (NCT01654562) to examine the short-term effects of Simvastatin on the vision of CHM male patients, evaluated by full-field scotopic threshold testing. The investigators hypothesized that they would see a reversible decrease in the dark-adapted vision in participants taking Simvastatin, however this study was terminated due to limited enrolment, with only 2 patients

recruited. It is unlikely that over such a short period of 5 weeks that a detectable change in full-field scotopic threshold testing or the other parameters, including microperimetry, would be a useful outcome metric. From this study, we would suggest a safer alternative for CHM patients would be to take fibrates to reduce cholesterol and overall lipid dysfunction. However, a trial of statin versus fibrate in those requiring treatment could be undertaken over a 12 month period measuring visual function parameters to assess for a decline, but numbers of patients would need to be high to achieve statistical significance in view of the intra- and inter-familial variability also seen with this disease.

Alterations in lipid catabolism are often linked to changes in oxidative stress. We observed mixed perturbations in the cysteine pathway that indicate altered demand for glutathione and may reflect a need to manage oxidative stress in CHM patients. While glutathione is typically not detected in plasma, loss of cysteine and associated dipeptide cysteinylglycine, and accumulation of hypotaurine are consistent with increased glutathione production. Additionally, differential changes in cysteinylglycine and 5-oxoproline support engagement of the glutathione cycle in CHM patients. This is consistent with our previous study showing elevated levels of oxidative stress (superoxide) in the retina of *chm*^{ru848} zebrafish mutant embryos (41). Oxidative damage can lead to a number of chronic diseases such as atherosclerosis, cardiovascular diseases, stroke, diabetics, rheumatoid arthritis, cancer, aging and other degenerative diseases in humans (42). Although we were unable to identify clear markers for these diseases in our study, exploring therapies focused on reducing oxidative stress levels may be beneficial in reducing any associated risk in CHM. Patients plasma revealed decreased levels of several known antioxidants, hence, diet

supplementation with antioxidant compounds like N-acetylcysteine (NAC) or even modulators of Nuclear factor erythroid 2-related factor 2 (NRF2), the “master regulator” of antioxidant response, could be of interest.

Increased oxidative stress may also contribute to CHM ocular manifestations, since it was found to cause retinal PR death and RPE atrophy in retinitis pigmentosa (RP), with a reduction in the reduced to oxidized glutathione ratio (GSH/GSSG) in aqueous humor (43). NAC was found to be an effective antioxidant in RP mouse models promoting cone survival and function (44) and a recent phase 1 clinical trial FIGUREHT-RP1 (NCT03999021 and NCT03063021) of orally administered NAC (maximum tolerated 1800mg twice a day) showed improvement of both cone function and best-corrected visual acuity (45). As delivered orally, NAC may help reduce the oxidative stress in the retina and the plasma of CHM patients with wider systemic benefit than just halting or slowing further sight loss.

Tryptophan metabolism results in the synthesis of neurotransmitters serotonin and melatonin, and via the kynurenine pathway produces nicotinamide, which is linked to inflammation and neurotoxicity of the central nervous system (CNS). We further examined metabolic markers of inflammation, however there was no strong evidence of involvement. Importantly, we observed a striking increase in serotonin levels in CHM patients. Serotonin regulates sleep, mood and behaviour and is also the precursor of melatonin, a powerful antioxidant essential for regulation of circadian rhythm (46). Serotonin is produced in the pineal gland and the gastrointestinal tract, but some can be produced in photoreceptors as a

precursor of melatonin, whose production is defined by the levels of light captured by the retina. Furthermore, serotonin acts as a neuromodulator in retinal physiology and photoreceptor survival (47). Serotonin is catabolised by action of monoamine oxygenase (MAO-A) and is reuptaken by serotonin transporter (SERT) – inhibitors of both enzymes increase serotonin levels and are used worldwide as antidepressants (47). Systemic high levels of serotonin can cause Serotonin syndrome, characterised by anxiety, muscle tremors or spasms, rapid heartbeat and high blood pressure (48). Mutations in MAO-A cause X-linked Brunner syndrome (OMIM 300615) which is characterised by increased monoamine levels like serotonin, dopamine and norepinephrine and leads to mild mental retardation, aggressive behaviour, sleep disorders and mood swings (49). Although serotonin levels in these syndromes are difficult to compare to CHM, it would be important to elucidate the link with elevated serotonin since there may be a subtle propensity for some of these features.

Serotonin can also regulate insulin secretion. Serotonylation is a post translational modification mechanism where transglutaminases add serotonin to the glutamine residues of GTPases, forming covalent bonds for activation of intracellular processes (50). Rab3a and Rab27, the latter a known target of REP1-dependent prenylation, are activated via this mechanism in the pancreas, which in turn promote glucose-mediated insulin secretion (51). Interestingly, we observed significant reduced levels of microbiome-related indoles, particularly indolepropionate, also resultant from tryptophan catabolism, which has antioxidant properties and was recently associated with lower risk of developing type 2 diabetes mellitus (52). No correlation has been reported between CHM

555 and diabetes, but these results suggest close monitoring of patients for insulin
556 insufficiency.
557
558 Melatonin levels could not be detected in this study, however, it has recently been
559 hypothesized as a potential antioxidant treatment for age-related macular
560 degeneration (AMD), by reducing oxidative stress, inflammation and apoptosis in
561 the retina (53). AMD aetiology has been compared to CHM and recent
562 metabolomic studies also revealed mitochondrial deficiency, as well as systemic
563 carnitine and glutamine pathway defects (54-56). Furthermore, Lains *et al*
564 showed decreased glycerophospholipids levels, particularly GPC, in AMD
565 plasma samples (56). CHM and AMD may share a common metabolome, hence,
566 the possible role of both serotonin and melatonin in the retina and RPE should
567 be further elucidated, possibly opening new therapeutic avenues.
568
569 The cytochrome P450 superfamily are a key family of monooxygenase enzymes
570 involved in metabolism of endogenous molecules, such as steroids and fatty
571 acids. Several of the metabolites that differed between CHM and control groups
572 were connected to liver cytochrome activity including reduced bilirubin and
573 increased urobilin. As heme levels were not significantly different, activity of heme
574 oxygenase I (HO-1), a rate limiting enzyme of heme catabolism, may have been
575 impaired. Interestingly, HO-1 was found to be increased after mevalonate
576 pathway inhibition using statins in mice macrophages; this change was
577 dependent on prenylation, since addition of FPP or GGPP partially reversed this
578 elevation (57).
579

Aside from the major metabolic perturbations discussed, there were other differentially identified metabolites of interest, such as ornithine, which was significantly increased (1.13-fold) in CHM. Ornithine is produced in the urea cycle by the splitting off of urea from arginine. Mutations in ornithine aminotransferase (OAT) cause gyrate atrophy (GA) (OMIM 258870), which is characterised by increased ornithine serum levels and has a similar clinical phenotype to CHM, with patients presenting with night blindness and progressive chorioretinal atrophy, eventually leading to blindness (58). Ornithine is toxic to the RPE and retina, thus lowering dietary intake can delay further retinal degeneration (59). No major systemic phenotypes are known to be associated with gyrate atrophy, but the increased ornithine levels in both disease groups suggest a close relationship between REP1 and OAT. Patients may benefit from dietary advice to reduce ornithine intake to prevent possible disease exacerbation.

Collectively, these results provide novel insights into the systemic derangements in CHM that occur due to disruption of REP1 activity. CHM is unlikely to be an isolated retinal dystrophy due to the ubiquitous expression of REP1. To date, accumulation of unprenylated Rab proteins is the only disease mechanism described in CHM, but this study proposes putative new enzymes, such as FALDH, cytochrome P450, monoamine or heme oxygenases, that could be targets of systemic REP1. The metabolic perturbations must be considered as pre-symptomatic risk factors for more chronic systemic involvement. Further long-term natural history studies are required into CHM and ageing to determine the prevalence of multisystemic manifestations. Therapeutic approaches could be developed for these modifiable risk factors, such as repurposing the S1P

receptor functional antagonist, fingolimod, to counter the effects of S1P accumulation in CHM. Use of in vitro and in vivo choroideremia disease models will also prove fundamental to establish the connection between the compounds described herein and REP1 function, providing new pathomechanisms in CHM, currently not completely understood.

Methods

CLINICAL EVALUATION

Twenty-five unrelated patients under Moorfields Eye Hospital NHS Foundation Trust, London, UK, with clinically diagnosed choroideremia and molecularly confirmed *CHM* hemizygous mutations were included in this study, together with 25 age- and gender- matched controls. A detailed ocular and medical history was taken with comprehensive ophthalmic examination as part of routine care (Supplementary Table 1). ETDRS best-corrected visual acuity (BCVA) was measured. Patients with clinical history of diabetes, hypercholesterolemia or drug history of taking statins or any other medications were a strict exclusion criteria.

ASSESSMENT OF DIETARY INTAKE

All CHM patients and control subjects were asked to complete a food frequency questionnaire (FFQ) on their average consumption of various foods and drinks over the past 12 months. The validated FFQ comprised a list of 147 food items and participants were asked to indicate their usual consumption from one of nine frequency categories ranging from “never or less than once per month” to “six or more times per day” (60). Individuals would have been excluded if their answers to >10 items had been left blank, but this was not true for any of the participants. Nutrients were calculated using the UK Nutrient Database (61).

SAMPLE COLLECTION

Blood plasma samples were collected from non-fasting CHM patients and age- and gender-matched healthy individuals (n=25 per group), between 9-11 am.

Plasma was extracted by centrifuging whole blood at 2000 rpm for 15 min at room temperature. Extracted plasma samples were aliquoted and stored at -80 °C. Samples that had not previously been thawed were shipped on dry ice to Metabolon Inc (Durham, NC, USA).

METABOLOMICS ANALYSIS

Blood plasma metabolite extractions for Ultrahigh Performance Liquid Chromatography-Tandem Mass Spectrometry (UPLC-MS/MS) were completed by Metabolon Inc (Durham, NC, USA), according to the protocol described in Supplementary Materials and Methods.

METABOLIC PATHWAY NETWORKS AND ANALYSIS

To visualise and analyse small molecules within relevant networks of metabolic pathways, the detected metabolites in CHM patient and healthy control study groups were subjected to MetaboLync pathway analysis (MPA) software (portal.metabolon.com). Significantly altered pathways were determined by completing pathway set enrichment analysis within MPA software which was determined by the following equation:

# of significant metabolites in pathway (k)/ total # of detected metabolites in pathway (m)/ total # of significant metabolites (n)/ total # of detected metabolites (N) or (k/m)/(n/N).

A pathway impact score greater than one indicated that the pathway contained a higher number of experimentally regulated compounds relative to the overall study in CHM patients relative to controls.

ZEBRAFISH HUSBANDRY

The wt AB (wildtype) and *chm*^{ru848} embryos were generated by natural pair-wise matings of identified heterozygous carriers. Embryos were raised at 28.5 °C on a 14-hr light/10-hr dark cycle in a 90mm petri dish containing aquarium water. The developmental stages are given in hours/days post-fertilization (hpf/dpf), according to morphological criteria (62).

SIMVASTATIN & FENOFIBRATE DOSING OF ZEBRAFISH

For all the dosing, the drugs were prepared in aquarium water. The *chm*^{ru848} mutant embryos were dechorionated at 10hpf and treated at 24hpf with either 0.3nM Simvastatin or 700nM Fenofibrate (63-65). The embryos were treated with a fresh dose of the drug(s) every 24 hours and as a positive control, an equal number of *chm*^{ru848} mutant embryos were kept in drug-free aquarium water. Survival of mutant larvae was recorded in days, n = 50 for each treatment group.

CHOLESTEROL ASSAY

Whole-body cholesterol was determined using the Amplex Red Cholesterol Assay kit (Life Technologies, CA, USA) according to the manufacturer's instructions. Pools of 5 wt AB and *chm*^{ru848} embryos per condition were collected and homogenized in sample buffer on ice. Cholesterol concentrations were measured using a TECAN microplate spectrofluorometer with an excitation wavelength of 545nm and an emission wavelength of 590nm. Concentrations were quantified using authentic cholesterol standards (provided in the kit) and estimated based on a gradient dilution of the cholesterol standards.

RETINAL HISTOLOGY & WHOLEMOUNT MORPHOLOGY

Retinal and wholemount morphology analyses were performed as previously described (21). All images were edited using ImageJ (NIH, USA).

LIPIDOMIC ANALYSIS OF ZEBRAFISH

Ten zebrafish were pooled for each sample (with 4 biological samples in total). Homogenisation to smooth emulsion was achieved by sonication of each pool in 100 µL water. Liquid-liquid extraction of this emulsion was performed similar to Izzi-Engbeaya et al (66). In brief, homogenised pool was mixed with isopropanol (IPA) spiked with internal standards 1:4 (V/V) in a microcentrifuge tube, incubated at 4°C with shaking at 1400 rpm for 2h, followed by centrifugation for 10 min at 3680g at 4°C, and the supernatant used for injection. LC-MS data were acquired as previously described (66). Feature extraction from LC-MS lipid positive and negative ion modes spectra was performed in XCMS (67) and by in-house scripts. Lipid annotation was achieved by tandem mass spectrometry acquisition (MSMS) followed by matching to inhouse and online databases. Measurement of pre-defined lipid of interests were detected, integrated and reported using an in-house open source package (https://doi.org/10.5281/zenodo.3523406).

STATISTICAL ANALYSIS

Mann-Whitney tests were used to compare age and dietary variables between patients and controls. Metabolite profiles in CHM patients and controls were quantified in terms of relative abundance and median scaled to 1. Following log transformation and imputation of missing values, if any, with the minimum observed value for each compound imputed, statistical analyses were performed

using ArrayStudio (Omicsoft, Cary, NC, USA) or R version 2.14.2 (https://www.r-project.org/). Metabolite profile distinctions between CHM patients and healthy individuals were evaluated by matched pair *t* tests. An estimate of the false discovery rate (*q* value) was calculated and a threshold of $q \leq 0.10$ was used to correct for false discovery of statistically significant compounds. Fold change (FC) was determined by dividing the relative abundance of each metabolite in the CHM patients blood plasma by the relative abundance of the metabolite in the blood plasma of healthy control individuals. FC values with $p \leq 0.05$ with $q \leq 0.10$ were considered statistically significant, while FC values with $0.05 < p < 0.10$ were considered as trending towards significance**.**

For zebrafish survival and cholesterol measurements, significance was calculated by One-way ANOVA. For lipidomic analysis, means and standard deviations were calculated using 10 fish per group (n=4). Statistical analysis was performed by One-way ANOVA using GraphPad Prism 8 v8.4.2 (GraphPad software, CA, USA; https://www.graphpad.com/).

Multivariate statistical analysis for lipidomic profiling of zebrafish (i.e. Principal Component Analysis (PCA)) was based upon the XCMS datasets from LC-MS spectra of zebrafish extracts and was performed using MATLAB based PLS_Toolbox version 8.7.1 (2019) (Eigenvector Research, Inc., WA, USA; http://www.eigenvector.com).

STUDY APPROVAL

The study protocol adhered to the tenets of the Declaration of Helsinki and received approval from Moorfields Eye Hospital NHS Foundation Trust and the

National Research Ethics Committee (REC12/LO/0141). Written informed consent was obtained from all participants prior to their inclusion in this study.

Zebrafish (wt AB and *chm*^{ru848}) were bred and maintained in the University College London animal facility according to standard protocols and the guidelines of the ARVO Statement for the Use of Animals in Ophthalmic and Vision Research (68).

AUTHOR CONTRIBUTIONS

DLC analysed the human and zebrafish data, performed statistical analysis and wrote the original draft; RR collected samples and wrote the first draft; DTW collected samples, performed zebrafish experiments and analysed data; AM and AA performed clinical evaluation of patients; VHvdS and PT performed target lipidomics and preliminary data analysis; NO contributed to data analysis; JS and AW conducted nutritional assessment of all participants; MM conducted the study, analysed data, acquired funding and wrote the manuscript. All authors reviewed and approved the manuscript before submission.

ACKNOWLEDGEMENTS

The authors are thankful to Metabolon Inc, particularly Gregory A. Michelotti, for metabolome profiling and assistance with data analysis, Dr Matthew Lewis and Dr Caroline Sands from the MRC-NIHR National Phenome Centre, Imperial College London, for input on the lipidomics experiments, and Eduardo Lima Cunha for helping with figure preparation. This work was supported by Wellcome Trust (grant number 205174/Z/16/Z), National Institute for Health Research (NIHR) Rare Diseases Translational Research Collaboration Award and the NIHR Biomedical Research Centre at Moorfields and UCL Institute of Ophthalmology, Choroideremia Research Foundation USA, Fight for Sight UK and Moorfields Eye Charity to MM. This work was also supported by the Medical Research Council and NIHR (grant number MC_PC_12025) and infrastructure support was provided by the National Institute for Health Research (NIHR) Imperial Biomedical Research Centre (BRC).

COMPETING INTERESTS

The authors have declared that no conflict of interest exists.

References

1. van den Hurk JA, Schwartz M, van Bokhoven H, van de Pol TJ, Bogerd L, Pinckers AJ, et al. Molecular basis of choroideremia (CHM): mutations involving the Rab escort protein-1 (REP-1) gene. *Human mutation.* 1997;9(2):110-7.
2. Mitsios A, Dubis AM, and Moosajee M. Choroideremia: from genetic and clinical phenotyping to gene therapy and future treatments. *Therapeutic advances in ophthalmology.* 2018;10:2515841418817490.
3. Moosajee M, Ramsden SC, Black GC, Seabra MC, and Webster AR. Clinical utility gene card for: choroideremia. *Eur J Hum Genet.* 2014;22(4).
4. Corbeel L, and Freson K. Rab proteins and Rab-associated proteins: major actors in the mechanism of protein-trafficking disorders. *European journal of pediatrics.* 2008;167(7):723-9.
5. Seabra MC, Ho YK, and Anant JS. Deficient geranylgeranylation of Ram/Rab27 in choroideremia. *The Journal of biological chemistry.* 1995;270(41):24420-7.
6. Seabra MC, Goldstein JL, Südhof TC, and Brown MS. Rab geranylgeranyl transferase. A multisubunit enzyme that prenylates GTP-binding proteins terminating in Cys-X-Cys or Cys-Cys. *The Journal of biological chemistry.* 1992;267(20):14497-503.
7. Cremers FP, Armstrong SA, Seabra MC, Brown MS, and Goldstein JL. REP-2, a Rab escort protein encoded by the choroideremia-like gene. *The Journal of biological chemistry.* 1994;269(3):2111-7.
8. Zhou Q, Weis E, Ye M, Benjaminy S, and MacDonald IM. An internet-based health survey on the co-morbidities of choroideremia patients. *Ophthalmic & physiological optics : the journal of the British College of Ophthalmic Opticians (Optometrists).* 2013;33(2):157-63.
9. Alizadeh J, Zeki AA, Mirzaei N, Tewary S, Rezaei Moghadam A, Glogowska A, et al. Mevalonate Cascade Inhibition by Simvastatin Induces the Intrinsic Apoptosis Pathway via Depletion of Isoprenoids in Tumor Cells. *Scientific reports.* 2017;7:44841.
10. Binnington B, Nguyen L, Kamani M, Hossain D, Marks DL, Budani M, et al. Inhibition of Rab prenylation by statins induces cellular glycosphingolipid remodeling. *Glycobiology.* 2016;26(2):166-80.
11. Kou X, Yang Y, Jiang X, Liu H, Sun F, Wang X, et al. Vorinostat and Simvastatin have synergistic effects on triple-negative breast cancer cells via abrogating Rab7 prenylation. *European journal of pharmacology.* 2017;813:161-71.
12. Jiao Z, Cai H, Long Y, Sirka OK, Padmanaban V, Ewald AJ, et al. Statin-induced GGPP depletion blocks macropinocytosis and starves cells with oncogenic defects. *Proceedings of the National Academy of Sciences of the United States of America.* 2020;117(8):4158-68.
13. Cheng Q, Gerald Robison W, and Samuel Zigler J. Geranylgeranyl pyrophosphate counteracts the cataractogenic effect of lovastatin on cultured rat lenses. *Experimental eye research.* 2002;75(5):603-9.
14. Zhang AY, Mysore N, Vali H, Koenekoop J, Cao SN, Li S, et al. Choroideremia Is a Systemic Disease With Lymphocyte Crystals and Plasma Lipid and RBC Membrane Abnormalities. *Investigative ophthalmology & visual science.* 2015;56(13):8158-65.
15. Radziwon A, Cho WJ, Szkotak A, Suh M, and MacDonald IM. Crystals and Fatty Acid Abnormalities Are Not Present in Circulating Cells From Choroideremia Patients. *Investigative ophthalmology & visual science.* 2018;59(11):4464-70.
16. Santoro MM. Zebrafish as a model to explore cell metabolism. *Trends in endocrinology and metabolism: TEM.* 2014;25(10):546-54.
17. Seth A, Stemple DL, and Barroso I. The emerging use of zebrafish to model metabolic disease. *Disease models & mechanisms.* 2013;6(5):1080-8.

18. Moosajee M, Tulloch M, Baron RA, Gregory-Evans CY, Pereira-Leal JB, and Seabra MC. Single choroideremia gene in nonmammalian vertebrates explains early embryonic lethality of the zebrafish model of choroideremia. *Investigative ophthalmology & visual science.* 2009;50(6):3009-16.
19. Starr CJ, Kappler JA, Chan DK, Kollmar R, and Hudspeth AJ. Mutation of the zebrafish choroideremia gene encoding Rab escort protein 1 devastates hair cells. *Proceedings of the National Academy of Sciences of the United States of America.* 2004;101(8):2572-7.
20. Hannun YA, and Obeid LM. Sphingolipids and their metabolism in physiology and disease. *Nature reviews Molecular cell biology.* 2018;19(3):175-91.
21. Moosajee M, Tracey-White D, Smart M, Weetall M, Torriano S, Kalatzis V, et al. Functional rescue of REP1 following treatment with PTC124 and novel derivative PTC-414 in human choroideremia fibroblasts and the nonsense-mediated zebrafish model. *Human molecular genetics.* 2016;25(16):3416-31.
22. Rakhshandehroo M, Knoch B, Müller M, and Kersten S. Peroxisome proliferator-activated receptor alpha target genes. *PPAR research.* 2010;2010.
23. Pralhada Rao R, Vaidyanathan N, Rengasamy M, Mammen Oommen A, Somaiya N, and Jagannath MR. Sphingolipid metabolic pathway: an overview of major roles played in human diseases. *Journal of lipids.* 2013;2013:178910.
24. Simón MV, Prado Spalm FH, Vera MS, and Rotstein NP. Sphingolipids as Emerging Mediators in Retina Degeneration. *Frontiers in cellular neuroscience.* 2019;13:246.
25. Weustenfeld M, Eidelpes R, Schmuth M, Rizzo WB, Zschocke J, and Keller MA. Genotype and phenotype variability in Sjögren-Larsson syndrome. *Human mutation.* 2019;40(2):177-86.
26. Nakahara K, Ohkuni A, Kitamura T, Abe K, Naganuma T, Ohno Y, et al. The Sjögren-Larsson syndrome gene encodes a hexadecenal dehydrogenase of the sphingosine 1-phosphate degradation pathway. *Molecular cell.* 2012;46(4):461-71.
27. Pinazo-Durán MD, Verdejo C, Azorín I, Renau-Piqueras J, and Iborra FJ. Colocalization of aldehyde dehydrogenases and Fe/NADPH-induced lipid peroxidation in tissue sections of rat retina. *Ophthalmic research.* 2000;32(2-3):61-8.
28. Fouzdar-Jain S, Suh DW, and Rizzo WB. Sjögren-Larsson syndrome: a complex metabolic disease with a distinctive ocular phenotype. *Ophthalmic genetics.* 2019;40(4):298-308.
29. Kitamura T, Naganuma T, Abe K, Nakahara K, Ohno Y, and Kihara A. Substrate specificity, plasma membrane localization, and lipid modification of the aldehyde dehydrogenase ALDH3B1. *Biochimica et biophysica acta.* 2013;1831(8):1395-401.
30. Kitamura T, Takagi S, Naganuma T, and Kihara A. Mouse aldehyde dehydrogenase ALDH3B2 is localized to lipid droplets via two C-terminal tryptophan residues and lipid modification. *The Biochemical journal.* 2015;465(1):79-87.
31. Vance JE, and Tasseva G. Formation and function of phosphatidylserine and phosphatidylethanolamine in mammalian cells. *Biochimica et biophysica acta.* 2013;1831(3):543-54.
32. Kim HY, Akbar M, and Kim YS. Phosphatidylserine-dependent neuroprotective signaling promoted by docosahexaenoic acid. *Prostaglandins, leukotrienes, and essential fatty acids.* 2010;82(4-6):165-72.
33. Ramanadham S, Ali T, Ashley JW, Bone RN, Hancock WD, and Lei X. Calcium-independent phospholipases A2 and their roles in biological processes and diseases. *Journal of lipid research.* 2015;56(9):1643-68.
34. Kolko M, Vohra R, Westlund van der Burght B, Poulsen K, and Nissen MH. Calcium-independent phospholipase A(2), group VIA, is critical for RPE cell survival. *Mol Vis.* 2014;20:511-21.

35. Zhan C, Wang J, and Kolko M. Diverse regulation of retinal pigment epithelium phagocytosis of photoreceptor outer segments by calcium-independent phospholipase A(2), group VIA and secretory phospholipase A(2), group IB. *Curr Eye Res.* 2012;37(10):930-40.
36. Tucker DE, Stewart A, Nallan L, Bendale P, Ghomashchi F, Gelb MH, et al. Group IVC cytosolic phospholipase A2gamma is farnesylated and palmitoylated in mammalian cells. *Journal of lipid research.* 2005;46(10):2122-33.
37. Rao PV, Robison WG, Jr., Bettelheim F, Lin LR, Reddy VN, and Zigler JS, Jr. Role of small GTP-binding proteins in lovastatin-induced cataracts. *Investigative ophthalmology & visual science.* 1997;38(11):2313-21.
38. Fujiwara K, Ikeda Y, Murakami Y, Funatsu J, Nakatake S, Tachibana T, et al. Risk Factors for Posterior Subcapsular Cataract in Retinitis Pigmentosa. *Investigative ophthalmology & visual science.* 2017;58(5):2534-7.
39. Murakami Y, Yoshida N, Ikeda Y, Nakatake S, Fujiwara K, Notomi S, et al. Relationship between aqueous flare and visual function in retinitis pigmentosa. *American journal of ophthalmology.* 2015;159(5):958-63.e1.
40. Borchman D, Cenedella RJ, and Lamba OP. Role of cholesterol in the structural order of lens membrane lipids. *Experimental eye research.* 1996;62(2):191-7.
41. Torriano S, Erkilic N, Baux D, Cereso N, De Luca V, Meunier I, et al. The effect of PTC124 on choroideremia fibroblasts and iPSC-derived RPE raises considerations for therapy. *Scientific reports.* 2018;8(1):8234.
42. Uttara B, Singh AV, Zamboni P, and Mahajan RT. Oxidative stress and neurodegenerative diseases: a review of upstream and downstream antioxidant therapeutic options. *Current neuropharmacology.* 2009;7(1):65-74.
43. Campochiaro PA, Strauss RW, Lu L, Hafiz G, Wolfson Y, Shah SM, et al. Is There Excess Oxidative Stress and Damage in Eyes of Patients with Retinitis Pigmentosa? *Antioxidants & redox signaling.* 2015;23(7):643-8.
44. Lee SY, Usui S, Zafar AB, Oveson BC, Jo YJ, Lu L, et al. N-Acetylcysteine promotes long-term survival of cones in a model of retinitis pigmentosa. *Journal of cellular physiology.* 2011;226(7):1843-9.
45. Campochiaro PA, Iftikhar M, Hafiz G, Akhlaq A, Tsai G, Wehling D, et al. Oral N-acetylcysteine improves cone function in retinitis pigmentosa patients in phase I trial. *The Journal of clinical investigation.* 2020;130(3):1527-41.
46. Yabut JM, Crane JD, Green AE, Keating DJ, Khan WI, and Steinberg GR. Emerging Roles for Serotonin in Regulating Metabolism: New Implications for an Ancient Molecule. *Endocrine reviews.* 2019;40(4):1092-107.
47. Masson J. Serotonin in retina. *Biochimie.* 2019;161:51-5.
48. Francescangeli J, Karamchandani K, Powell M, and Bonavia A. The Serotonin Syndrome: From Molecular Mechanisms to Clinical Practice. *International journal of molecular sciences.* 2019;20(9).
49. Brunner HG, Nelen MR, van Zandvoort P, Abeling NG, van Gennip AH, Wolters EC, et al. X-linked borderline mental retardation with prominent behavioral disturbance: phenotype, genetic localization, and evidence for disturbed monoamine metabolism. *American journal of human genetics.* 1993;52(6):1032-9.
50. Walther DJ, Peter JU, Winter S, Höltje M, Paulmann N, Grohmann M, et al. Serotonylation of small GTPases is a signal transduction pathway that triggers platelet alpha-granule release. *Cell.* 2003;115(7):851-62.
51. Paulmann N, Grohmann M, Voigt JP, Bert B, Vowinckel J, Bader M, et al. Intracellular serotonin modulates insulin secretion from pancreatic beta-cells by protein serotonylation. *PLoS biology.* 2009;7(10):e1000229.
52. de Mello VD, Paananen J, Lindström J, Lankinen MA, Shi L, Kuusisto J, et al. Indolepropionic acid and novel lipid metabolites are associated with a lower risk of

type 2 diabetes in the Finnish Diabetes Prevention Study. *Scientific reports.* 2017;7:46337.

53. Blasiak J, Reiter RJ, and Kaarniranta K. Melatonin in Retinal Physiology and Pathology: The Case of Age-Related Macular Degeneration. *Oxidative medicine and cellular longevity.* 2016;2016:6819736.

54. Chao de la Barca JM, Rondet-Courbis B, Ferré M, Muller J, Buisset A, Leruez S, et al. A Plasma Metabolomic Profiling of Exudative Age-Related Macular Degeneration Showing Carnosine and Mitochondrial Deficiencies. *Journal of clinical medicine.* 2020;9(3).

55. Kersten E, Dammeier S, Ajana S, Groenewoud JMM, Codrea M, Klose F, et al. Metabolomics in serum of patients with non-advanced age-related macular degeneration reveals aberrations in the glutamine pathway. *PloS one.* 2019;14(6):e0218457.

56. Laíns I, Chung W, Kelly RS, Gil J, Marques M, Barreto P, et al. Human Plasma Metabolomics in Age-Related Macular Degeneration: Meta-Analysis of Two Cohorts. *Metabolites.* 2019;9(7).

57. Chen JC, Huang KC, and Lin WW. HMG-CoA reductase inhibitors upregulate heme oxygenase-1 expression in murine RAW264.7 macrophages via ERK, p38 MAPK and protein kinase G pathways. *Cellular signalling.* 2006;18(1):32-9.

58. Kennaway NG, Weleber RG, and Buist NR. Gyrate atrophy of choroid and retina: deficient activity of ornithine ketoacid aminotransferase in cultured skin fibroblasts. *The New England journal of medicine.* 1977;297(21):1180.

59. Kaiser-Kupfer MI, de Monasterio FM, Valle D, Walser M, and Brusilow S. Gyrate atrophy of the choroid and retina: improved visual function following reduction of plasma ornithine by diet. *Science.* 1980;210(4474):1128-31.

60. Welch AA, Luben R, Khaw KT, and Bingham SA. The CAFE computer program for nutritional analysis of the EPIC-Norfolk food frequency questionnaire and identification of extreme nutrient values. *Journal of human nutrition and dietetics : the official journal of the British Dietetic Association.* 2005;18(2):99-116.

61. Bingham SA, Gill C, Welch A, Cassidy A, Runswick SA, Oakes S, et al. Validation of dietary assessment methods in the UK arm of EPIC using weighed records, and 24-hour urinary nitrogen and potassium and serum vitamin C and carotenoids as biomarkers. *International journal of epidemiology.* 1997;26 Suppl 1:S137-51.

62. Kimmel CB, Ballard WW, Kimmel SR, Ullmann B, and Schilling TF. Stages of embryonic development of the zebrafish. *Developmental dynamics : an official publication of the American Association of Anatomists.* 1995;203(3):253-310.

63. Ashikawa Y, Nishimura Y, Okabe S, Sasagawa S, Murakami S, Yuge M, et al. Activation of Sterol Regulatory Element Binding Factors by Fenofibrate and Gemfibrozil Stimulates Myelination in Zebrafish. *Frontiers in pharmacology.* 2016;7:206.

64. Campos LM, Rios EA, Guapyassu L, Midlej V, Atella GC, Herculano-Houzel S, et al. Alterations in zebrafish development induced by simvastatin: Comprehensive morphological and physiological study, focusing on muscle. *Experimental biology and medicine (Maywood, NJ).* 2016;241(17):1950-60.

65. Campos LM, Rios EA, Midlej V, Atella GC, Herculano-Houzel S, Benchimol M, et al. Structural analysis of alterations in zebrafish muscle differentiation induced by simvastatin and their recovery with cholesterol. *The journal of histochemistry and cytochemistry : official journal of the Histochemistry Society.* 2015;63(6):427-37.

66. Izzi-Engbeaya C, Comninos AN, Clarke SA, Jomard A, Yang L, Jones S, et al. The effects of kisspeptin on β-cell function, serum metabolites and appetite in humans. *Diabetes, obesity & metabolism.* 2018;20(12):2800-10.

973 67. Smith CA, Want EJ, O'Maille G, Abagyan R, and Siuzdak G. XCMS: processing mass
974 spectrometry data for metabolite profiling using nonlinear peak alignment, matching,
975 and identification. *Analytical chemistry.* 2006;78(3):779-87.
976 68. Westerfield M. *The Zebrafish Book: A Guide for the Laboratory Use of Zebrafish (Danio*
977 *Rerio).* University of Oregon Press; 2000.

978

979

FIGURE LEGENDS

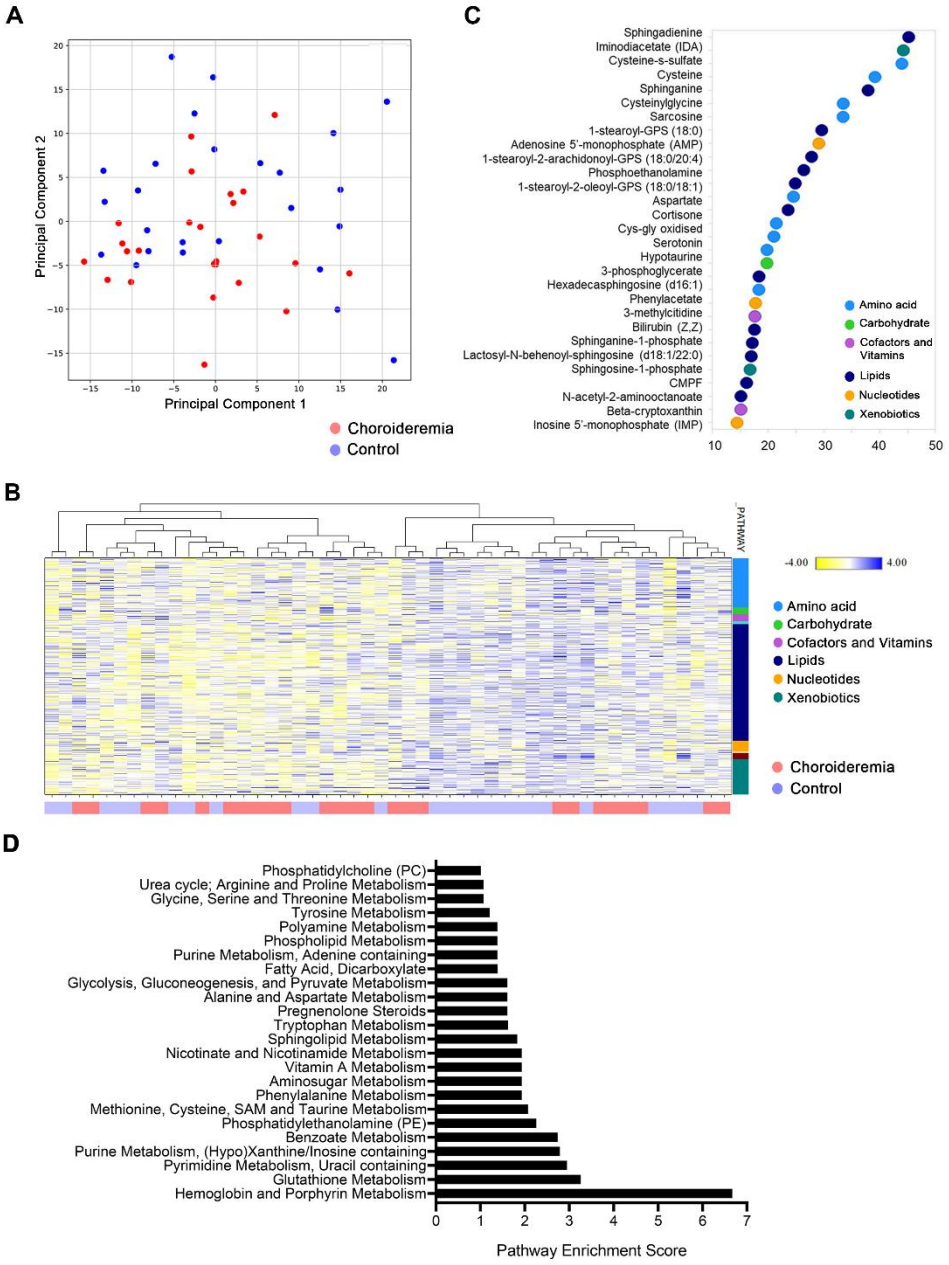

Figure 1. Global metabolomic analysis of choroideremia (CHM) patients versus age- and gender-matched controls (A) Principal component analysis (PCA). Control and CHM samples are represented as blue and red circles, respectively (n=25 each group). (B) Cluster analysis of control and CHM samples show no clear separation between groups. (C) Top 30 metabolites detected by Random forest analysis based on importance to group separation. (D) Pathway analysis calculated using MetaboLync pathway analysis (MPA) software. Pathways with MPA Score higher than 1 were considered.

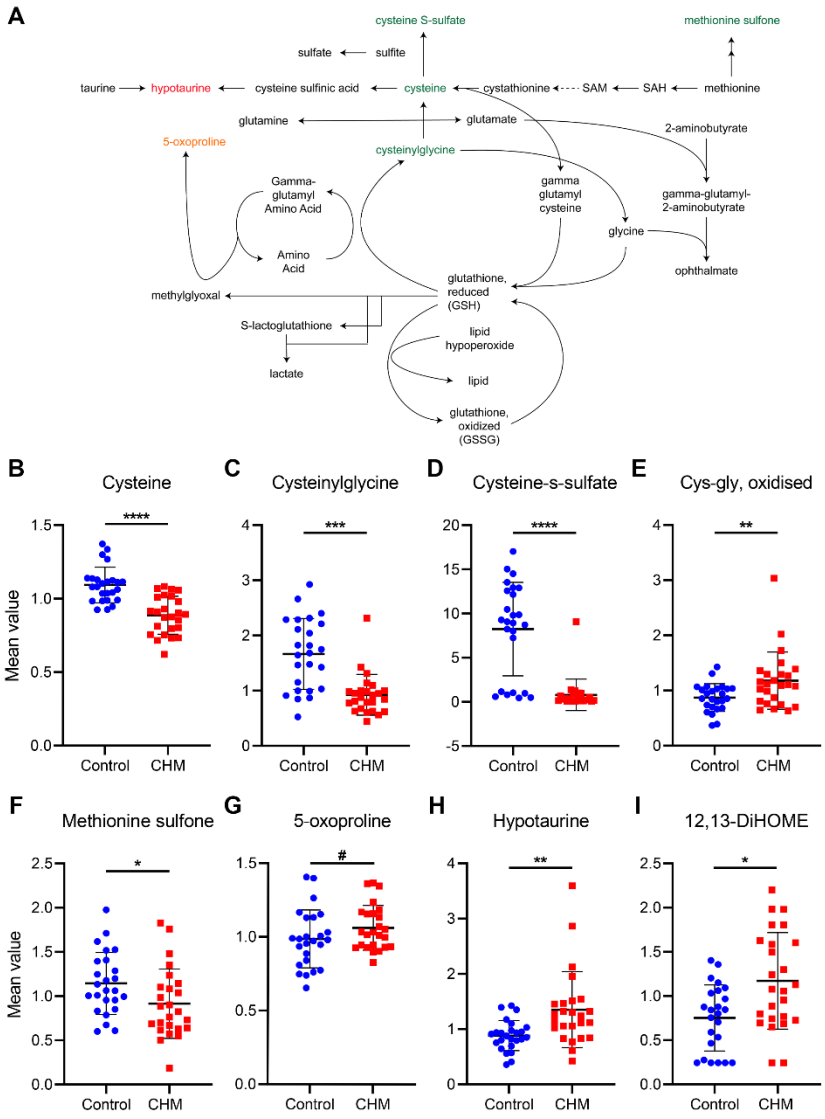

990

991 **Figure 2. CHM patients exhibit evidence of increased oxidative stress**. (A) Schematic of the
992 glutathione metabolism pathway, where several compounds were found to be increased (red) or
993 decreased (green) in CHM patients compared to controls. Significantly altered metabolites ($p \leq$
994 0.05) are highlighted in bold, to distinguish from those with trending significance ($0.05 < p \leq 0.1$).
995 (B-I) Scatter dot plots of specific metabolites indicating the mean ± SD levels in CHM patient
996 samples (red) and control samples (blue) (n=25). *p* value was determined using matched pair *t*
997 tests: # $0.05 < p \leq 0.1$, * $p \leq 0.05$, ** $p \leq 0.01$, *** $p \leq 0.001$, **** $p \leq 0.0001$.

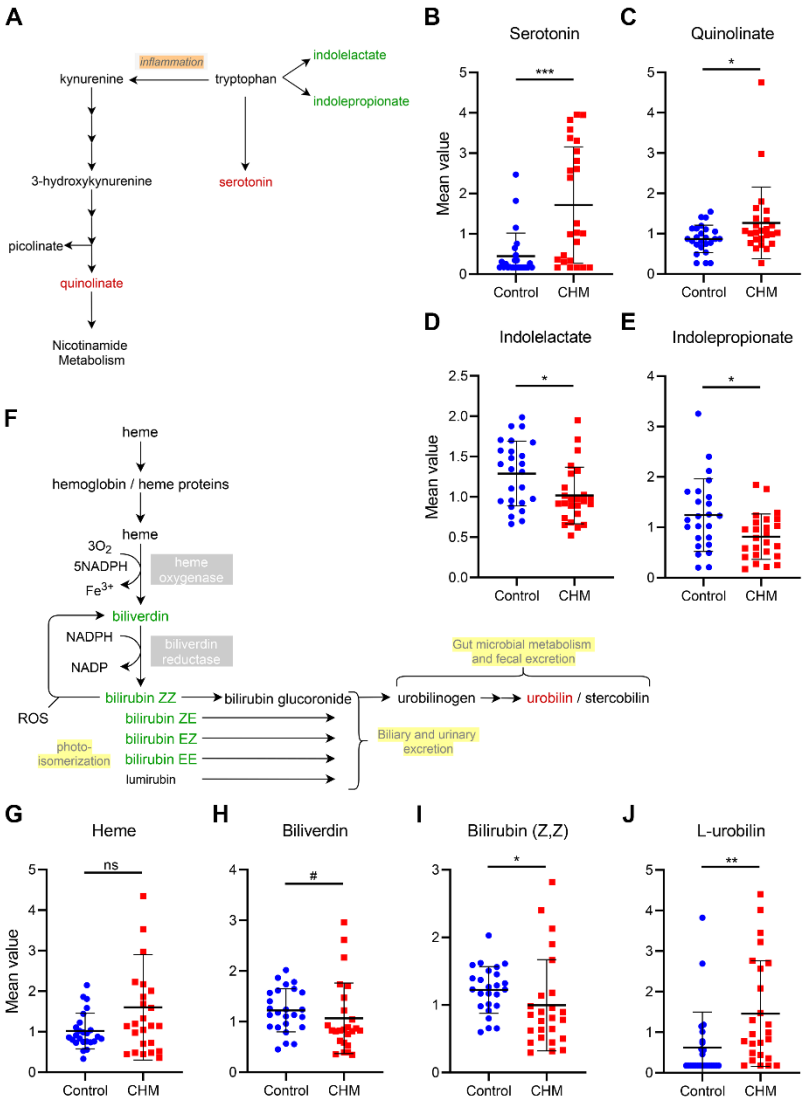

998

999 **Figure 3. Alterations in tryptophan and haemoglobin metabolism pathways in CHM**
1000 **patients**. (A) Pathway schematics and altered metabolites in tryptophan metabolism with
1001 decreased metabolites in green and increased in red. (B-E) Scatter dot plots of altered
1002 metabolites showing control (blue) and CHM (red) groups with mean ± SD (n=25). (F) Schematic
1003 representation in the Haemoglobin/ Heme metabolism pathway with decreased metabolites
1004 shown in green and increased metabolites in red. (G-J) Scatter dot plots of altered metabolites
1005 showing control (blue) and CHM (red) groups with mean ± SD (n=25). *p* value was determined
1006 using matched pair *t* tests: *ns* not significant, # $0.05 < p \leq 0.1$, * $p \leq 0.05$, ** $p \leq 0.01$, *** $p \leq 0.001$.
1007

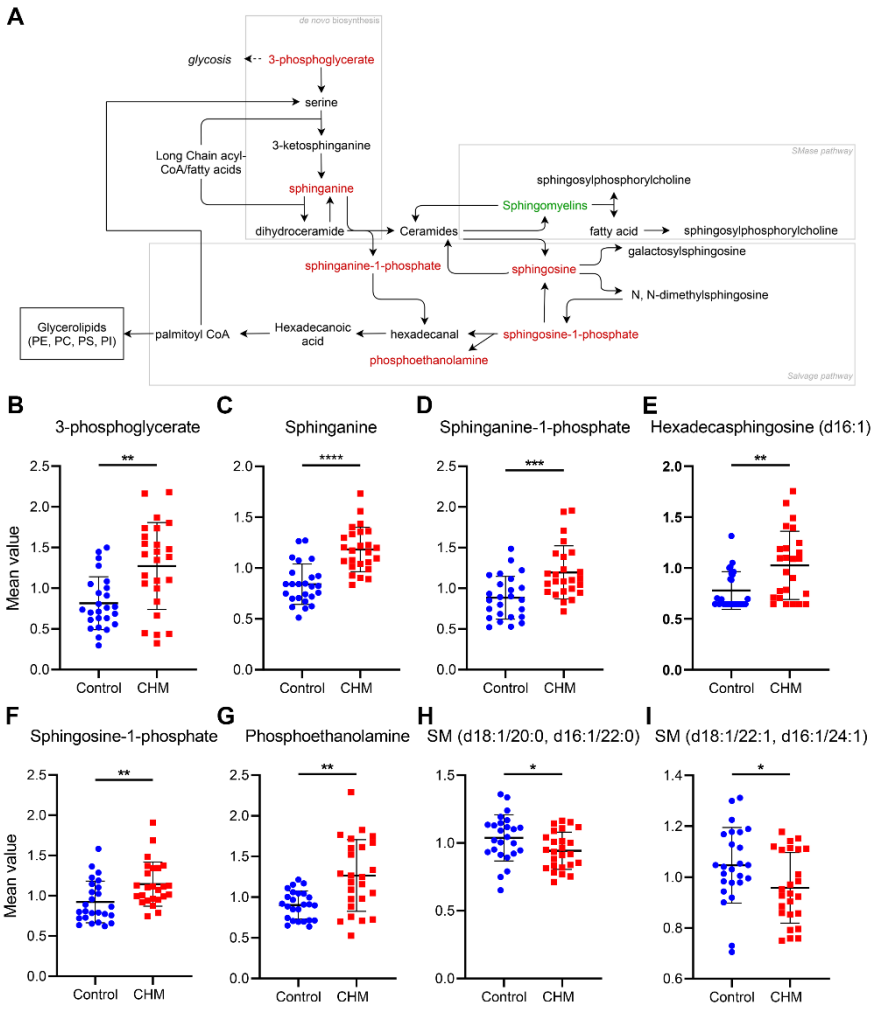

Figure 4. Disturbance of sphingolipid metabolism in CHM patients. A) General sphingolipid metabolism pathway with compounds differentially detected in CHM patients highlighted in red (increased) or green (decreased) compared to control levels. B-I) Scatter dot plots of key metabolite levels in both control (blue) and choroideremia (red) plasma samples. Lines indicate mean ± SD (n=25). *p* value was determined using matched pair *t* tests: * $p \leq 0.05$, ** $p \leq 0.01$, *** $p \leq 0.001$, **** $p \leq 0.0001$. Abbreviations: SM, sphingomyelin.

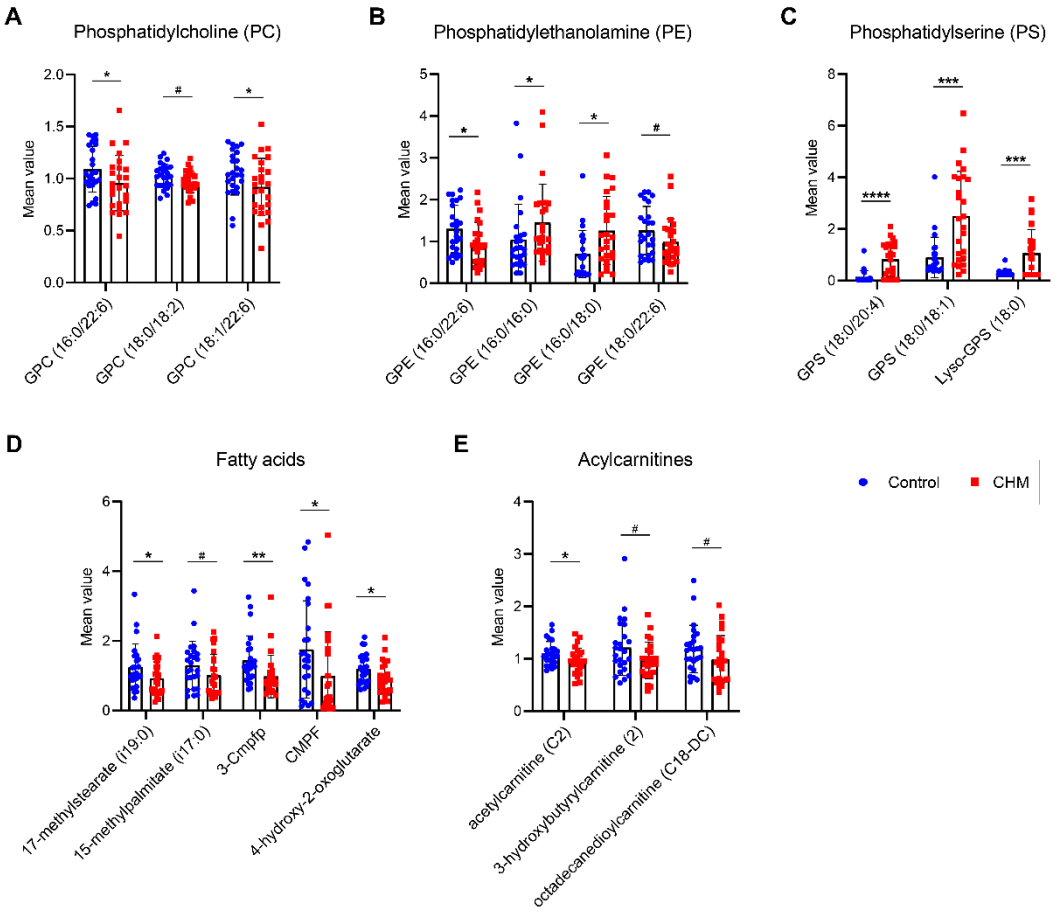

Figure 5. Metabolites involved in lipid metabolism subclasses differentially detected in CHM patients. Bars represent mean ± SD of control (blue) and choroideremia (red) plasma samples (n=25). *p* value was determined using matched pair *t* tests: * $p \leq 0.05$, ** $p \leq 0.01$, *** $p \leq 0.001$, **** $p \leq 0.0001$. Abbreviations: GPC, glycerophosphocholine; GPE, gylcerophosphoethanolamine; GPS, glycerophosphoserine; 3-Cmpfp, 3-carboxy-4-methyl-5-pentyl-2-furanpropionate; CMPF, 3-carboxy-4-methyl-5-propyl-2-furanpropanoate.

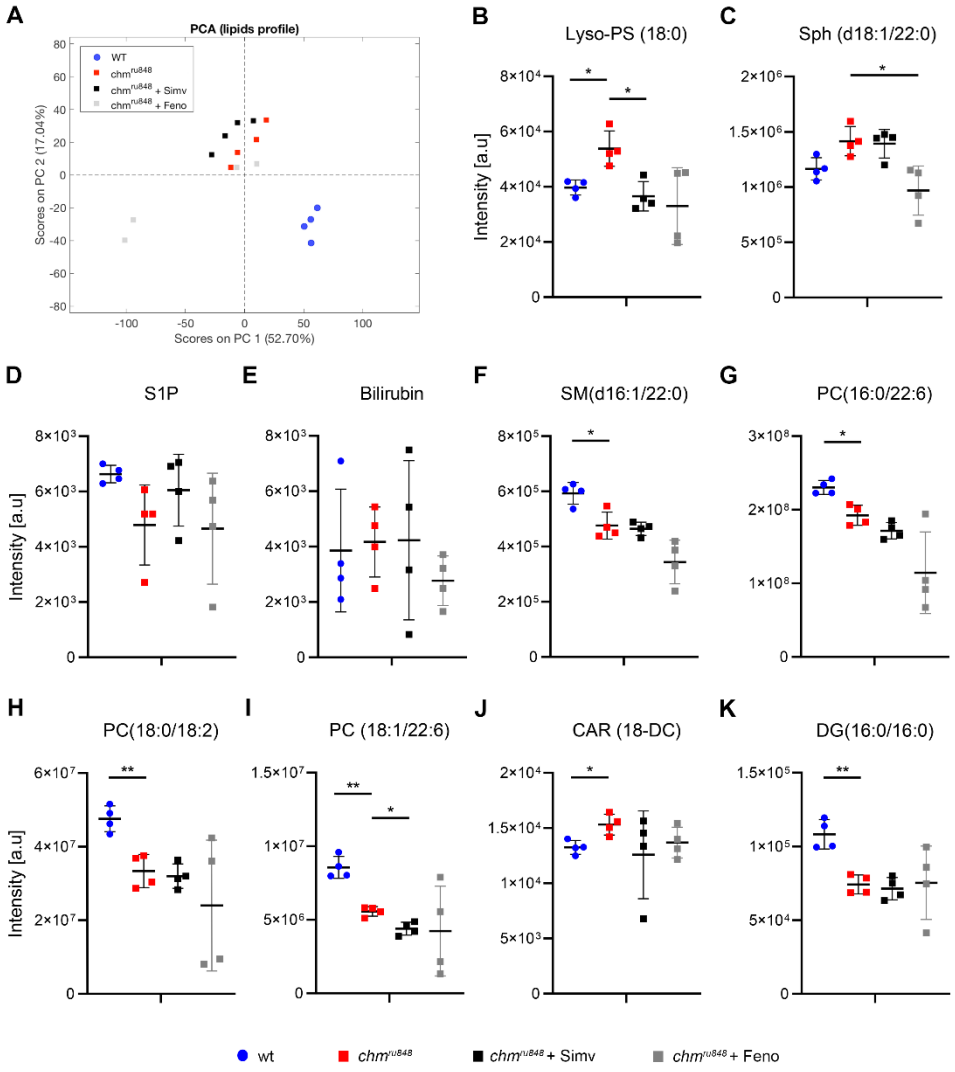

1023

1024 **Figure 6. Lipidomic profiles of zebrafish: wildtype (wt), *chm* mutant (*chm*^{ru848}) untreated,**

1025 **treated with Simvastatin or Fenofibrate.** (A) PCA analysis of day 6 *chm* ^{ru848} mutant fish

1026 untreated (red squares), treated with 0.3nM Simvastatin (black squares) or 700nM Fenofibrate

1027 (grey squares), compared to wt fish (blue circles). (B-K) Scatter dot plots with key metabolites

1028 shared with human plasma metabolites and respective levels detected in all groups. Lines indicate

1029 mean ± SD (n=4, 10 fish per group). *p* value was determined using One-way ANOVA * $p \leq 0.05$,

1030 ** $p \leq 0.01$. Abbreviations: a.u., arbitrary units; Lyso-PS, lysophosphoserine/ 1-stearoyl-GPS;

1031 Sph(d18:1/22:0), lactosyl-N-behenoyl-sphingosine; S1P, sphingosine-1-phosphate; CAR,

1032 carnitine; PC, phosphatidylcholine; SM, sphingomyelin.

1033

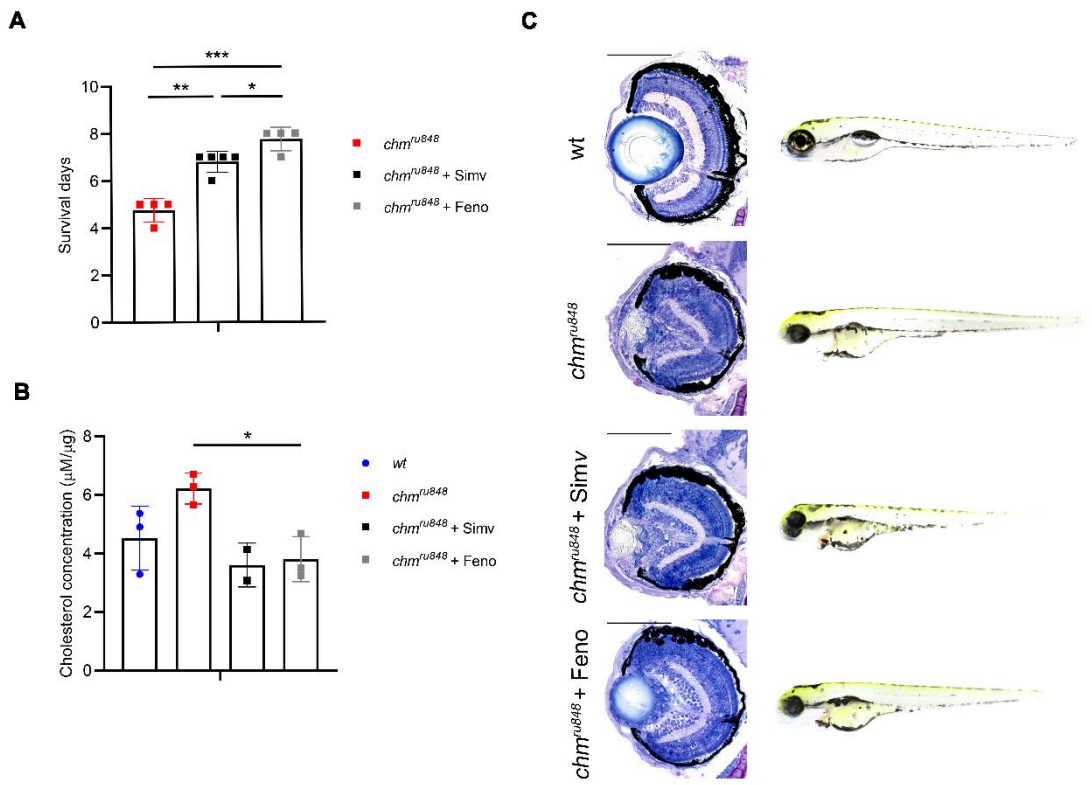

Figure 7. Characterisation of *chm*^{ru848} zebrafish treated daily with 0.3nM Simvastatin or 700nM Fenofibrate from 24 hours post fertilisation. (A) Survival days of *chm*^{ru848} fish untreated (red), treated with Simvastatin (black) and Fenofibrate (grey) (n=4, 50 fish per group). (B) Average levels of cholesterol (µM per µg of protein) in wt fish (blue circles), and *chm*^{ru848} zebrafish untreated (red squares), treated with Simvastatin (black squares) and with Fenofibrate (grey squares) at 6 days post fertilisation (dpf) (n ≥ 2, 5 fish per condition). Data represent mean ± SD. (C) Retinal sections and wholemount morphology of wt, untreated *chm*^{ru848} fish, and *chm*^{ru848} fish treated with Simvastatin and Fenofibrate at 6dpf. Scale bar 100µm. *p* value was determined using One-way ANOVA. * $p \leq 0.05$, ** $p \leq 0.01$, *** $p \leq 0.001$.